Marine Micropaleontology 88–89 (2012) 65–76

Contents lists available at SciVerse ScienceDirect

Marine Micropaleontology

journal homepage: www.elsevier.com/locate/marmicro

# Central Arctic paleoceanography for the last 50 kyr based on ostracode faunal assemblages

Robert K. Poirier [a,*], Thomas M. Cronin [a], William M. Briggs Jr. [b,1], Rowan Lockwood [c]

[a] U.S. Geological Survey, MS926A 12201 Sunrise Valley Dr. Reston, VA 20192, United States
[b] Institute of Arctic and Alpine Research, Campus Box 450, University of Colorado, Boulder, CO 80309-0450, United States
[c] Department of Geology, P.O. Box 8795, College of William and Mary, Williamsburg, VA 23187, United States

ARTICLE INFO

*Article history:*
Received 12 August 2011
Received in revised form 12 March 2012
Accepted 19 March 2012
Available online 30 March 2012

*Keywords:*
Arctic Ocean
Ostracode
Paleoceanography
Paleoclimatology
Dansgaard–Oeschger
Heinrich
Age models
MIS 1
MIS 2
MIS 3

ABSTRACT

The paleoceanography of the central Arctic Ocean was reconstructed for the last 50 kyr (Marine Isotope Stages (MIS) 1–3) based on ostracode assemblages from 21 $^{14}$C-dated sediment cores from the Mendeleev, Lomonosov, and Gakkel Ridges. Arctic sediments deposited during the Holocene interglacial period (MIS 1), the Bølling–Allerød, and larger interstadial Dansgaard–Oeschger (DO) events (3–4, 8, and 12) contain abundant *Cytheropteron* spp., *Henryhowella asperrima*, and *Krithe* spp. at intermediate/deep-depths (~1000 to 3000 m). These assemblages suggest a ventilated deep, Arctic Ocean water mass similar to the modern Arctic Ocean Deep Water (AODW) during these time periods. In contrast, sediment deposited during stadial events corresponding to Heinrich events 1, 2, 3, and 4, (also possibly the Younger Dryas; YD), contain abundant *Polycope* spp. (60–80%) suggesting a greater influence of the Atlantic Layer (AL) on the Arctic Intermediate Water (AIW) and AODW. Reduced sea-ice during the early Holocene, the last deglacial, and MIS 3 interstadials is indicated by the reoccurrence of *Acetabulastoma arcticum*, an epipelagic species that is parasitic on sea-ice dwelling amphipods. One hypothesis to explain these oceanographic changes during longer stadial events, particularly within the last glacial period (MIS 2), involves sluggish ocean circulation, thicker sea-ice cover, and a deeper halocline with ocean exchange between Greenland Sea and Arctic Ocean deep-water through the Fram Strait.

Published by Elsevier B.V.

## 1. Introduction

The Arctic Ocean influences global climate and ocean circulation through the contribution of Arctic deep-water to the global thermohaline system (Aagaard et al., 1985, 1991; Rudels and Quadfasel, 1991; Aagaard and Carmack, 1994; Anderson et al., 1994; Meincke et al., 1997; Rudels et al., 2004). Many climate and oceanographic studies suggest that large temperature changes in the Arctic are currently occurring in shallow to intermediate water depths (McLaughlin et al., 2009; Polyakov et al., 2011; Spielhagen et al., 2011) as well as declining annual Arctic perennial sea-ice cover (Stroeve et al., 2007a,b; Comiso et al., 2008; Rothrock et al., 2008; Kwok and Rothrock, 2009). Large changes in Arctic Ocean circulation during the last 50 kyr have also been hypothesized from sediment core proxy records (Stein et al., 1994a,b; Cronin et al., 1995; Jakobsson et al., 2001; Nørgaard-Pederson et al., 2003; Polyak et al., 2004; Spielhagen et al., 2004, 2005; Wollenburg et al., 2004; Darby et al., 2006; Polyak et al., 2010). Some studies postulate large changes in the Arctic Ocean during interstadial and stadial events of the last glacial period covering the last 50 kyr, including MIS 2 and 3 (Spielhagen et al., 2004, 2005; Darby et al., 2006). However, many aspects of Arctic Ocean circulation during past climate change cycles remain poorly understood due to low sedimentation rates, limited sediment chronology, and complex oceanographic changes.

This study investigates changes in late Quaternary benthic ostracode faunas from sediment cores in the central Arctic Ocean and applies them to the reconstruction of intermediate and deep-water circulation during the last 50 kyr. The focus is on several key ostracode taxa that act as faunal tracers of major water masses and sea ice conditions, and were recovered from 21 deep-sea sediment cores from the Gakkel, Lomonosov, and Mendeleev Ridges, and the Morris Jesup Rise. These sites cover a large part of the central Arctic Ocean and are presently located within the modern Arctic Intermediate Water (AIW), Canada Basin Deep Water (CBDW) and the Eurasian Basin Deep Water (EBDW) masses (Fig. 1). In addition to studying faunal changes, we attempted to improve Arctic chronology by recalibrating published radiocarbon dates from 22 cores and obtaining new radiocarbon dates from four cores. These recalibrated dates should help to improve interpretations of Arctic oceanography during glacial/interglacial cycles, as well as millennial-scale climate events (Dansgaard–Oeschger interstadial and Heinrich stadial events).

* Corresponding author. Tel.: +1 434 203 9304.
*E-mail address:* rkpoir@udel.edu (R.K. Poirier).
[1] Now at NAMPRO, 3000 Colorado Ave., A201, Boulder, CO, 80303, United States.

0377-8398/$ – see front matter. Published by Elsevier B.V.
doi:10.1016/j.marmicro.2012.03.004

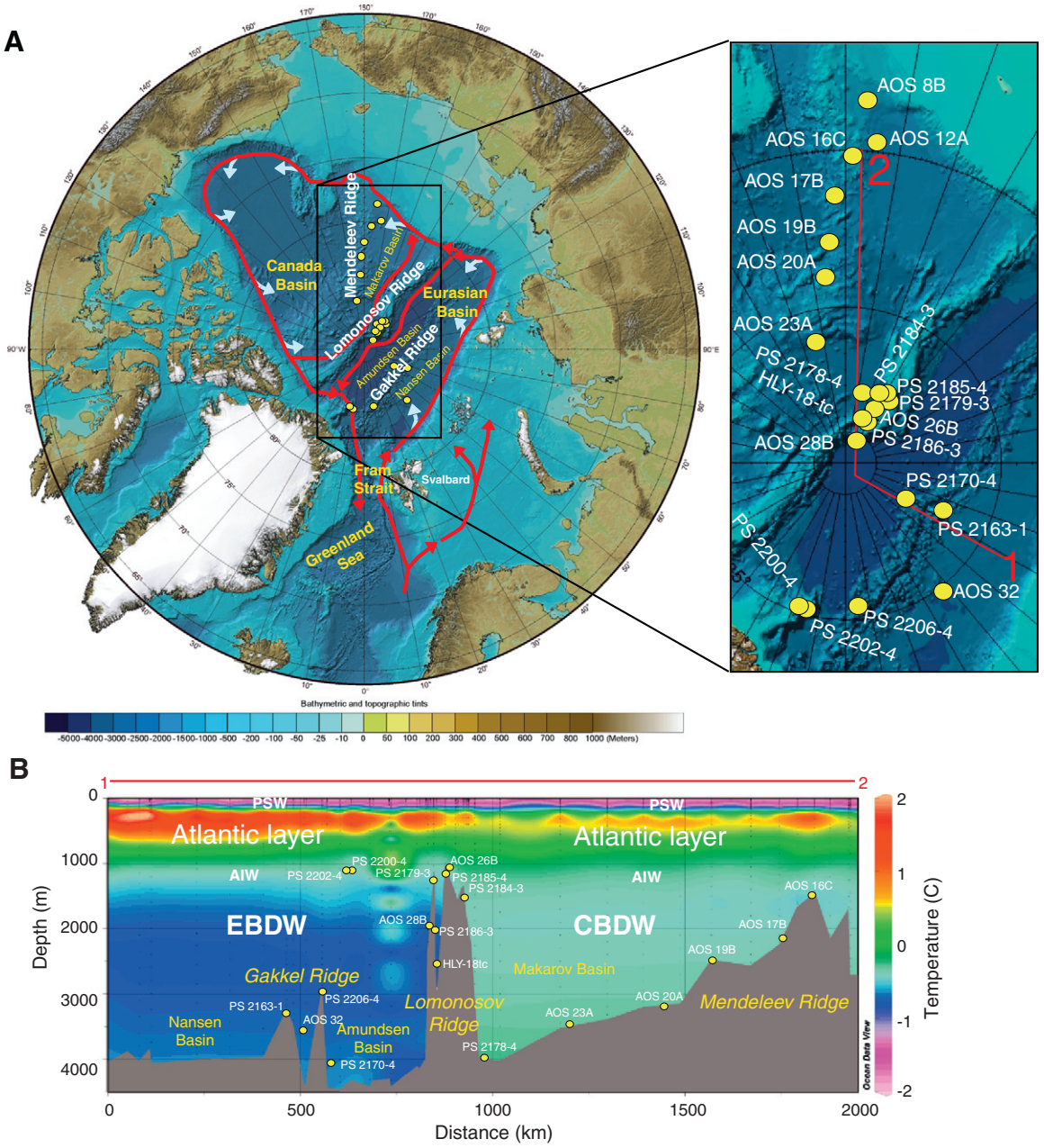


**Fig. 1.** A. International Bathymetric Chart of the Arctic Ocean with the 21 core sites from this study (from Jakobsson et al., 2008). See supplemental information on the location of the core sites in Table 1. Also shown is the generalized circulation of the Atlantic Layer (AL) within the Arctic Ocean (red). The blue arrows demonstrate brine formation on the continental shelves. B. Cross sectional temperature profile of the modern Arctic Ocean with cores from this study marked (AOS94B8B and AOS94B12A not shown). (For interpretation of the references to color in this figure legend, the reader is referred to the web version of this article.)

## 2. Background

### 2.1. Modern Arctic oceanography

Today, the central Arctic Ocean is stratified into four primary layers: the Polar Surface Water (PSW) (Jones, 2001; Rudels et al., 2004) (also known as the Polar Mixed Layer, or PML), the Atlantic Layer (AL), the Arctic Intermediate Water (AIW), and the Arctic Ocean Deep Water (AODW) (Aagaard and Carmack, 1989; Anderson et al., 1994). The AODW is separated into the Canada Basin Deep Water (CBDW) and the Eurasian Basin Deep Water (EBDW) by the Lomonosov Ridge (Fig. 1B). The PSW (~0 to 50 m), primarily sourced from glacial melt and transpolar currents from the Siberian shelf to the Fram Strait and Beaufort Sea Gyre, is relatively cold (0 to −2 °C) and fresh (~32 to 34 ppt) (Fig. 1B) (Anderson and Jones, 1992; Jones, 2001; Karcher and Oberhuber, 2002; Rudels et al., 2004; Woodgate et al., 2007). An ~100 m deep halocline separates the PSW from the underlying AL (Fig. 1B) (Rudels et al., 1996). Today, the AL occurs from ~200 to 1000 m and is warmer (≥0 °C as defined by Rudels et al. (2004)), and more saline (~34.3 to 34.75 ppt), than the overlying PSW (Fig. 1B). The core of the AL, between 300 and 500 m water depths, and can reach temperatures exceeding 2 °C (Fig. 1) (Rudels et al., 2004). The AIW, which lies beneath and is influenced by the AL (Fig. 1B), refers to a water mass at depths of ~1000 to 1500 m in the Eurasian Basin and up to ~2000 m in the Canada Basin. This water mass is also referred to as the upper-AODW (upper-CBDW, upper-EBDW). The AL appears to influence the temperature and salinity of the modern AIW (~−0.5 to 0 °C; ~34.6 to 34.8 ppt), and as we discuss below, probably experienced large changes during the last 50 kyr (Fig. 1). The AODW fills the deep Arctic Basins beneath the AIW, at

water depths of >2000 m in the Canada Basin, and >1500 m in the Eurasian Basin (Fig. 1). Overall, the AODW is colder and more saline (thus denser) than the AIW (CBDW of −0.5 to −0.3 °C and 34.95 ppt; and in EBDW of −1.0 to −0.6 °C and 34.93 ppt) (Fig. 1B).

The following simplified description of the intermediate and deep-water circulation in the Arctic Ocean draws on the studies of Rudels and Quadfasel (1991), Anderson et al. (1994), Jones et al. (1995a, 1995b), Meincke et al. (1997), Karcher and Oberhuber (2002), and Rudels et al. (1994, 1996, 2004). The Atlantic Layer enters the Fram Strait area at a rate of 5–8 Sv ($1\ Sv = 1 \times 10^6\ m^3\ s^{-1}$) (Worthington, 1970; McCartney and Talley, 1984); ~1 Sv enters the Central Arctic Ocean (Rudels, 1987; Bourke et al., 1988) (Fig. 1A). In the Arctic Ocean, the AL continues along the Eurasian continental shelf until it is split at the Lomonosov Ridge. One branch of the AL diverts pole-ward along the eastern side of the Lomonosov Ridge, and the other crosses over into the Canadian Basin. Here, the AL continues along the continental slope of the Canada Basin, until it eventually returns to the Lomonosov Ridge. The AL splits again, as part of it re-circulates along the western side of the Lomonosov Ridge, flowing once more along the continental shelf rim of the Canadian Basin, and eventually rejoins the eastern-Lomonosov branch, and ultimately exits the Arctic via the Fram Strait (Fig. 1A). Within the Canada Basin, the AL entrains to greater depths as it reaches the continental slope via mixing with shelf brines, influencing the AIW, and eventually the CBDW. This causes the CBDW (>~2000 m) to be warmer (−0.5 to −0.3 °C) than the EBDW (>~1500 m; −1.0 to −0.6 °C), and increases the distribution of the Atlantic Layer's heat into the Canada Basin (Fig. 1B).

The branch of the AL on the eastern Lomonosov Ridge travels pole-ward at depths of ~200–1500 m with minimal influence from continental shelf brines. Beneath it is the colder and denser Eurasian Basin Deep Water (EBDW) (Fig. 1B). This portion of the AL eventually rejoins the branch that circulated through the Canada Basin, and together they exit the Arctic Ocean through the Fram Strait. The CBDW and the EBDW also combine at the southern-most reach of the Lomonosov Ridge, near Greenland, to form the AODW, which then flows through the Fram Strait into the Greenland Sea (Fig. 1). Here, the AODW contributes to the GSDW, which ultimately influences the formation of North Atlantic Deep Water (NADW) via convection.

### 2.2. Arctic Ocean ostracodes

Arctic marine ostracodes have been the subject of many prior studies based on living material and surface sediment collections. References used in this study for ostracode taxonomy and ecology include Joy and Clark (1977), Whatley and Coles (1987), Cronin et al. (1994, 1995, 2010), Whatley et al. (1995), Jones et al. (1998, 1999), and Stepanova et al. (2003, 2007, 2010). Five of the most common deep-sea ostracode taxa were chosen for paleoceanographic reconstruction: *Krithe* spp., *Polycope* spp., *Henryhowella asperrima* s.l. (Reuss), *Cytheropteron* spp., and *Acetabulastoma arcticum* (Schornikov). The taxon *Krithe* spp. includes *K. glacialis* (Brady, Crosskey, and Robertson) and *K. minima* (Coles, Whatley, and Moguilevsky), which are both indicative of cold, well-ventilated water typically found today in highest abundance within the AODW (Joy and Clark, 1977; Cronin et al., 1994, 1995). Of the two species, *K. minima* is much less common than *K. glacialis* and typically lives near the eastern Arctic margin at slightly shallower depths than *K. glacialis*. *H. asperrima* is found in highest abundance within the AODW and is hypothesized to be indicative of cold, well-ventilated water. The genus *Polycope* (Sars) includes nine Arctic species, which typically occur together in sediments in contact with the AIW (Joy and Clark, 1977; Cronin et al., 1994, 1995). This taxon is often associated with high productivity, probably warmer temperatures, and appears to represent an opportunistic group of species, often dominating up to 80–90% of fossil assemblages. The group of *Cytheropteron* spp. includes the intermediate/deep-water (>1000 m) species *C. alatum* (Sars), *C. bronwynae* (Joy and Clark), *C. carolinae* (Whatley and Coles), and *C. hamatum* (Sars). These four species typically dominate assemblages in the AODW (CBDW and EBDW) (Joy and Clark, 1977; Cronin et al., 1994, 1995). The species *A. arcticum* lives as a parasite on pelagic, sympagic amphipods, which inhabit sub-sea-ice habitats, and have been used as a perennial sea-ice indicator (Cronin et al., 2010).

### 2.3. Climate events of the last 50 kyr

Climate variability from the last 50 kyr included many abrupt stadial periods such as Heinrich (H) events (Heinrich, 1988; Bond et al., 1992; Andrews, 1998; Hemming, 2004) and Dansgaard–Oeschger (DO) stadial–interstadial cycles (Dansgaard et al., 1993; Clark et al., 2002). It has been suggested that Heinrich events during the last glacial possibly weakened NADW formation (Keigwin and Lehman, 1994; Sarnthein et al., 1994; Elliot et al., 2002). The current Holocene interglacial also shows oceanographic variability, but it is smaller in scale than stadial/interstadial variation during the last glacial (Kaufman et al., 2004).

## 3. Materials and methods

Ostracode faunas were studied at 1 cm intervals in 21 sediment cores (Table 1; all faunal data available online at the National Climatic Data Center: http://www.ncdc.noaa.gov/paleo/paleo.html). Species were identified and counted in each sample and the relative frequencies were computed for all taxa within each sample as percent abundance of the total assemblage (abundance henceforth). Overall, 151,100 specimens were counted (single valves and carapaces were counted as one specimen), with an average of 282 specimens per sample. We analyzed ten multi-cores from the *Arctic 91* Expedition (PS 2163–1, PS 2170–4, PS 2178–4, PS 2179–3, PS 2184–3, PS 2185–4, PS 2186–3, PS 2200–4, PS 2202–4, and PS 2206–4), ten box-cores from the *AOS SR96-1994* cruise (AOS94B8B, AOS94B12A, AOS94B16C, AOS94B17B, AOS94B19B, AOS94B20A, AOS94B23A, AOS94B26B, AOS94B28B, and AOS94B32), and one trigger-core from the 2005 *HOTRAX* Expedition (HLY0503-18tc) (Fig. 1; Table 1).

Various grain sizes have been examined in prior ostracode studies from the Arctic, most commonly either ≥150 μm, or ≥125 μm. The current study was the culmination of several years of research and incorporates faunal analyses using both the ≥125 μm size fraction (195 samples), and the ≥150 μm size fraction (226 samples). In order to assess whether the size-fraction used introduced a bias into the assemblage data, we compared assemblages picked from both size-fractions in samples from core AOS94B8B. The resulting abundances of the five key taxa in the ≥150 μm fell within the 95% confidence limits for those from the ≥125 μm size fraction (Table 2). The insignificant differences between assemblages from the ≥125 and ≥150 μm size fractions is likely because ostracodes grow by molting, and adult specimens and most pre-adults (A-1, A-2 instars) for most species are preserved in the ≥150 μm fraction (one exception is *Microcythere medistriata* (Joy and Clark, 1977), a rare, small species which on average constitutes ~1.7% of our assemblages in either size fraction).

We calculated 95% error bars for the relative abundance in each sample, as well as for the composite faunal curve discussed below. This was accomplished by applying the algorithm for a binomial probability distribution provided by Raup (1991) to the relative frequency of each species, and the total specimen count for each sample at a given core depth (Percent Error Bars program, S. Holland pers. comm. 2011). These error bars allowed us to identify statistically significant increases or decreases in taxon abundances through time.

### 3.1. Chronology and reservoir corrections

Radiocarbon dating provides the primary age control on the MIS 3 through 1 interval in the Arctic sediments. We compiled a total of 181 previously published dates from 22 Arctic cores (Darby et al.,

**Table 1**
Cruise and core site information for 21 cores in this study. Sedimentation rates from age models derived from radiocarbon dates from each core. (N = number of dates; nI = number of infinite dates; ! represents 1 unused radiocarbon date (likely due to bioturbation or dating error)).

| | | | | | | | Sedimentation rates | | | | | | | | | | | | | |
|---|---|---|---|---|---|---|---|---|---|---|---|---|---|---|---|---|---|---|---|---|
| | | | | | | | Holocene | | | Post-LGM | | | | 40ka-LGM | | | Pre-40ka | | | | |
| Year | Cruise | Core | Latitude | Longitude | WD (m) | Location | N | Sed rate (cm/ka) | Core depths (cm) | N | Sed rate (cm/ka) | Core depths (cm) | LGM depth (cm) | N | Sed rate (cm/ka) | Core depths (cm) | N | Sed rate (cm/ka) | Core depths (cm) | nI dates | Base age (ka); (base depth) |
| 1994 | *AOS SR96-1994* | AOS94B8B | 78.13 | −176.75 | 1031 | Mendeleev Ridge | 4 | 2.10 | 0–11 | 0 | 2.10 | 15–18 | 18 | 0 | 0.85 | 18–20 | 3 | 0.85 | 20–41 | | 52.12 (41) |
| 1994 | *AOS SR96-1994* | AOS94B12A | 79.99 | −174.29 | 1683 | Mendeleev Ridge | 3 | 0.84 | 0–9 | 0 | 0.84 | 9–11 | 11 | 0 | 3.78 | 11–12 | 4 | 3.78 | 12–40 | | 47.19 (40) |
| 1994 | *AOS SR96-1994* | AOS94B16C | 80.34 | −178.71 | 1568 | Mendeleev Ridge | 2 | 0.56 | 0–11 | 3 | 2.36 | 11–14 | 14 | 3 | 0.81 | 14–21 | 4 | 1.30 | 21–35 | 1 | 50.60 (35) |
| 1994 | *AOS SR96-1994* | AOS94B17B | 81.27 | 178.97 | 2117 | Mendeleev Ridge | 8 | 1.40 | 0–11 | 6 | 1.40 | 11–16 | 16 | 3 | 0.36 | 20–26 | 3! | 2.19 | 26–39 | | 45.83 (39) |
| 1994 | *AOS SR96-1994* | AOS94B19B | 82.45 | 175.76 | 2414 | Mendeleev Ridge | 1 | 0.54 | 0–6 | 3 | 0.54 | 6–8 | 8 | 4 | 0.39 | 8–15 | 5! | 2.69 | 15–37 | | 50.42 (37) |
| 1994 | *AOS SR96-1994* | AOS94B20A | 83.17 | 174.11 | 3120 | Mendeleev Ridge | 3! | 0.56 | 0–5 | 1 | 0.56 | 5–10 | 10 | 3! | 1.22 | 10–22 | 3 | 1.22 | 22–39 | | 54.08 (39) |
| 1994 | *AOS SR96-1994* | AOS94B23A | 85.90 | −166.83 | 3475 | Makarov abyss | | | | | | | | | | | | | | | |
| 1994 | *AOS SR96-1994* | AOS94B26B | 88.06 | −142.98 | 1020 | Lomonosov Ridge | 1 | 0.47 | 0–3 | 1 | 0.47 | 3–6 | 6 | 1 | 0.25 | 6–12 | 1 | 0.25 | 12–16 | | 48.40 (16) |
| 1994 | *AOS SR96-1994* | AOS94B28B | 88.87 | −140.18 | 1990 | Lomonosov Ridge | 5 | 1.08 | 0–12 | 2! | 1.08 | 12–18 | 18 | 2 | 0.21 | 18–22 | 5!! | 2.68 | 22–35 | | 47.06 (35) |
| 1994 | *AOS SR96-1994* | AOS94B32 | 85.72 | 37.74 | 3450 | Gakkel Ridge | | | | | | | | | | | | | | | |
| 1991 | Arctic 91 | PS 2163-1 | 86.24 | −59.22 | 3040 | Gakkel Ridge | 1 | 0.58 | 0–6 | 1 | 0.58 | 6–10 | 10 | 0 | 0.75 | 10–23 | 0 | 0.75 | 23–27 | 2 | 43.33 (27) |
| 1991 | Arctic 91 | PS 2170-4 | 87.60 | 60.90 | 4083 | Amundsen abyss | 1 | 0.76 | 0–8 | 1 | 0.76 | 8–15 | 15 | 1 | 0.35 | 15–21 | 1 | 0.35 | 21–25 | | 52.44 (26) |
| 1991 | Arctic 91 | PS 2178-4 | 88.02 | 159.59 | 4008 | Makarov abyss | | | | | | | | | | | | | | | |
| 1991 | Arctic 91 | PS 2179-3 | 87.75 | −138.16 | 1228 | Lomonosov Ridge | 3 | 1.37 | 0–12 | 0 | 1.37 | 12–17 | 17 | 1 | 0.48 | 17–26 | 0 | 0.48 | 26–24 | | 35.20 (24) |
| 1991 | Arctic 91 | PS 2184-3 | 87.61 | −148.25 | 1674 | Lomonosov Ridge | 1 | 0.68 | 0–3 | 1 | 0.68 | 3–7 | 7 | 1 | 0.26 | 7–11 | 0 | 0.26 | 11–14 | | 47.51 (14) |
| 1991 | Arctic 91 | PS 2185-4 | 87.53 | −144.48 | 1051 | Lomonosov Ridge | 8 | 0.79 | 0–9 | 3 | 0.39 | 9–13 | 13 | 4 | 0.21 | 13–19 | 0 | 1.16 | 19–25 | | 45.03 (25) |
| 1991 | Arctic 91 | PS 2186-3 | 88.51 | −140.36 | 2004 | Lomonosov Ridge | 2 | 1.18 | 0–11 | n/a | n/a | n/a | 11 | 1 | 0.67 | 11–23 | 1 | 0.67 | 23–26 | | 43.23 (26) |
| 1991 | Arctic 91 | PS 2200-4 | 85.33 | −14.00 | 1074 | Morris Jessup Rise | 1 | 0.51 | 0–3 | 1 | 0.51 | 3–6 | 6 | 3 | 0.30 | 6–12 | 0 | 0.30 | 12–16 | 1 | 53.25 (16) |
| 1991 | Arctic 91 | PS 2202-4 | 85.10 | −14.40 | 1084 | Morris Jessup Rise | | | | | | | | | | | | | | | |
| 1991 | Arctic 91 | PS 2206-4 | 85.28 | −2.51 | 2993 | Gakkel Ridge | 2 | 0.64 | 0–7 | 1 | 0.64 | 7–14 | 14 | 1 | 0.36 | 14–20 | 0 | 0.36 | 20–29 | | 62.70 (29) |
| 2005 | *HOTRAX* | HLY0503-18-tc | 88.45 | 146.68 | 2654 | Lomonosov Ridge | 8 | 2.35 | 0–20 | 5 | 2.35 | 20–27 | 27 | 3 | 2.14 | 27–57 | 1! | 2.14 | 57–63 | 5 | 42.63 (63) |

**Table 2**
Table providing the results of the ≥125 μm and ≥150 μm size fraction comparisons within core AOS94B8B for *Acetabulastoma arcticum*, *Cytheropteron* spp., *Krithe* spp., and *Polycope* spp. Each taxon's abundance data from both size fractions, and upper and lower limits for the ≥125 μm size fraction based on 95% confidence intervals are given. Results show no data bias between the two size fractions.

| | | *Acetabulastoma arcticum* | | | | *Cytheropteron* spp. | | | | *Krithe* spp. | | | | *Polycope* spp. | | | |
|---|---|---|---|---|---|---|---|---|---|---|---|---|---|---|---|---|---|
| Depth (cm) | Age (ka) | ≥125 μm (abundance) | Lower limit | Upper limit | ≥150 μm (abundance) | ≥125 μm (abundance) | Lower limit | Upper limit | ≥150 μm (abundance) | ≥125 μm (abundance) | Lower limit | Upper limit | ≥150 μm (abundance) | ≥125 μm (abundance) | Lower limit | Upper limit | ≥150 μm (abundance) |
| 2.5 | 4.93 | 0.75 | 0.00 | 2.00 | 1.12 | 23.13 | 18.20 | 28.30 | 22.91 | 17.91 | 13.40 | 22.60 | 19.55 | 41.79 | 35.90 | 47.70 | 45.25 |
| 3.5 | 5.41 | 1.94 | 0.50 | 3.60 | 0.52 | 25.16 | 20.40 | 30.10 | 25.65 | 21.61 | 17.10 | 26.30 | 22.51 | 37.74 | 32.40 | 43.20 | 42.93 |
| 4.5 | 5.88 | 1.42 | 0.00 | 3.20 | 1.91 | 34.12 | 27.80 | 40.60 | 30.57 | 28.44 | 22.40 | 34.60 | 29.30 | 28.44 | 22.40 | 34.60 | 30.57 |
| 6.5 | 6.83 | 0.00 | 0.00 | 4.50 | 0.00 | 32.24 | 24.90 | 39.80 | 31.15 | 27.63 | 20.70 | 34.90 | 29.51 | 30.92 | 23.70 | 38.40 | 31.97 |
| 7.5 | 7.31 | 1.09 | 0.00 | 2.90 | 0.84 | 34.24 | 27.50 | 41.20 | 34.45 | 22.83 | 16.90 | 29.00 | 23.53 | 33.15 | 26.40 | 40.00 | 35.29 |
| 8.5 | 7.78 | 1.32 | 0.00 | 3.50 | 1.01 | 27.81 | 20.80 | 35.10 | 27.27 | 16.56 | 10.80 | 22.70 | 17.17 | 45.70 | 37.80 | 53.70 | 48.48 |
| 9.5 | 8.26 | 0.00 | 0.00 | 4.40 | 0.00 | 21.85 | 14.70 | 29.50 | 21.05 | 14.29 | 8.30 | 20.90 | 11.58 | 55.46 | 46.50 | 64.30 | 57.89 |
| 11.5 | 9.21 | 1.57 | 0.00 | 3.60 | 2.19 | 31.94 | 25.40 | 38.60 | 28.47 | 12.57 | 8.10 | 17.50 | 13.87 | 45.03 | 38.00 | 52.10 | 45.26 |
| 12.5 | 9.68 | 1.29 | 0.00 | 3.40 | 0.80 | 34.19 | 26.80 | 41.80 | 37.60 | 17.42 | 11.60 | 23.60 | 14.40 | 38.71 | 31.10 | 46.50 | 39.20 |
| 13.5 | 10.16 | 2.48 | 0.70 | 4.60 | 1.80 | 33.88 | 28.00 | 39.90 | 32.34 | 22.73 | 17.60 | 28.10 | 23.95 | 28.93 | 23.30 | 34.70 | 31.74 |
| 14.5 | 10.63 | 1.82 | 0.00 | 4.10 | 0.85 | 35.15 | 27.90 | 42.50 | 32.20 | 13.94 | 8.90 | 19.40 | 13.56 | 38.79 | 31.40 | 46.30 | 44.07 |
| 16.5 | 11.59 | 5.26 | 0.00 | 17.60 | 0.00 | 42.11 | 20.00 | 64.80 | 47.06 | 21.05 | 3.90 | 41.00 | 17.65 | 31.58 | 11.40 | 53.70 | 35.29 |
| 17.5 | 12.06 | 2.13 | 0.00 | 7.20 | 2.56 | 38.30 | 24.70 | 52.40 | 41.03 | 0.00 | 1.60 | 16.60 | 0.00 | 55.32 | 41.00 | 69.40 | 53.85 |
| 18.5 | 26.25 | 4.35 | 0.00 | 11.30 | 0.00 | 39.13 | 25.30 | 53.40 | 44.74 | 0.00 | 1.60 | 16.90 | 0.00 | 47.83 | 33.50 | 62.30 | 44.74 |
| 19.5 | 27.43 | 1.25 | 0.00 | 4.20 | 0.00 | 37.50 | 27.00 | 48.20 | 31.48 | 0.00 | 0.90 | 9.70 | 0.00 | 55.00 | 44.00 | 65.80 | 64.81 |
| 21.5 | 29.78 | 0.00 | 0.00 | 11.30 | 0.00 | 40.00 | 22.70 | 57.90 | 40.91 | 0.00 | 2.50 | 25.90 | 0.00 | 60.00 | 42.10 | 77.30 | 59.09 |
| 22.5 | 30.95 | 1.25 | 0.00 | 4.20 | 0.00 | 30.00 | 20.20 | 40.30 | 28.85 | 1.25 | 0.00 | 4.20 | 1.92 | 58.75 | 47.80 | 69.40 | 61.54 |
| 23.5 | 32.13 | 0.48 | 0.00 | 1.60 | 0.00 | 15.87 | 11.00 | 21.00 | 15.03 | 0.48 | 0.00 | 1.60 | 0.00 | 75.96 | 70.00 | 81.70 | 77.12 |
| 24.5 | 33.30 | 2.23 | 0.60 | 4.20 | 0.68 | 17.84 | 13.40 | 22.50 | 11.56 | 0.74 | 0.00 | 2.00 | 0.00 | 74.72 | 69.40 | 79.80 | 82.31 |
| 26.5 | 35.66 | 3.73 | 1.10 | 6.90 | 2.83 | 22.36 | 16.10 | 29.00 | 21.70 | 2.48 | 0.40 | 5.20 | 1.89 | 65.22 | 57.80 | 72.50 | 65.09 |
| 27.5 | 36.83 | 2.46 | 0.80 | 4.40 | 2.75 | 19.30 | 14.80 | 24.00 | 15.93 | 4.91 | 2.60 | 7.60 | 6.04 | 65.26 | 59.70 | 70.70 | 64.84 |
| 28.5 | 38.01 | 1.05 | 0.00 | 2.80 | 0.00 | 20.00 | 14.50 | 25.80 | 18.11 | 3.16 | 0.90 | 5.90 | 3.94 | 68.95 | 62.30 | 75.40 | 70.87 |
| 29.5 | 39.18 | 4.55 | 1.00 | 8.80 | 3.61 | 30.00 | 21.60 | 38.70 | 28.92 | 3.64 | 0.60 | 7.50 | 3.61 | 58.18 | 48.90 | 67.40 | 60.24 |
| 31.5 | 41.54 | 5.38 | 1.90 | 9.60 | 6.25 | 16.92 | 10.70 | 23.60 | 19.79 | 0.00 | 0.50 | 6.40 | 0.00 | 68.46 | 60.40 | 76.30 | 62.50 |
| 32.5 | 42.71 | 2.70 | 0.00 | 7.10 | 0.00 | 22.97 | 13.70 | 32.90 | 21.43 | 2.70 | 0.00 | 7.10 | 3.57 | 59.46 | 48.20 | 70.60 | 66.07 |
| 33.5 | 43.89 | 2.05 | 0.30 | 4.30 | 0.95 | 16.41 | 11.40 | 21.80 | 17.14 | 6.67 | 3.40 | 10.40 | 8.57 | 72.82 | 66.50 | 79.00 | 70.48 |
| 34.5 | 45.06 | 1.94 | 0.90 | 3.20 | 1.75 | 16.61 | 13.60 | 19.70 | 14.91 | 9.19 | 6.90 | 11.60 | 11.40 | 66.25 | 62.30 | 70.10 | 66.96 |
| | | | | | Avg. Δ = 0.82 | | | | Avg. Δ = 0.62 | | | | Avg. Δ = 0.62 | | | | Avg. Δ = 1.85 |

**Table 3**
List of new radiocarbon dates obtained in this study obtained from *N. pachyderma*. Calibrated ages calculated using reservoir values from Hanslik et al. (2010).

| Core | Sample depth (cm) | Lab number | Uncalibrated $^{14}$C age (BP) | Error ± | Calibrated $^{14}$C age (BP) | Error (2 std dev) ± |
|---|---|---|---|---|---|---|
| PS 2179-3 | 2.5 | NOSAMS 85337 | 4140 | 30 | 3790 | 101 |
| | 6.5 | NOSAMS 85338 | 7420 | 45 | 7590 | 89 |
| | 11.5 | NOSAMS 85339 | 9690 | 40 | 10,250 | 99 |
| | 23.5 | NOSAMS 85340 | 32,200 | 220 | 35,200 | 433 |
| AOS94B8B | 0.5 | NOSAMS 85341 | 3990 | 30 | 3600 | 101 |
| | 4.5 | NOSAMS 85342 | 7710 | 30 | 7870 | 75 |
| | 10.5 | NOSAMS 85343 | 8630 | 35 | 8880 | 122 |
| | 14.5 | NOSAMS 85344 | 8630 | 35 | 8880 | 122 |
| | 25.5 | NOSAMS 85345 | 35,900 | 200 | 39,530 | 715 |
| | 33.5 | NOSAMS 85346 | 46,000 | 530 | 47,810 | 1496 |
| | 40.5 | NOSAMS 85347 | 40,300 | 260 | 43,150 | 538 |
| AOS94B20A | 5.5 | NOSAMS 85348 | 12,000 | 55 | 12,510 | 138 |
| | 10.5 | NOSAMS 85349 | 27,800 | 130 | 31,030 | 212 |
| | 15.5 | NOSAMS 85350 | 43,700 | 340 | 45,570 | 613 |
| | 20.5 | NOSAMS 85351 | 43,000 | 420 | 45,110 | 667 |
| | 30.5 | NOSAMS 85352 | 27,800 | 120 | 31,040 | 199 |
| AOS94B26B | 0.5 | NOSAMS 85354 | 4440 | 30 | 4210 | 120 |
| | 5.5 | NOSAMS 85355 | 13,950 | 45 | 14,780 | 354 |

1997; Nørgaard-Pedersen et al., 1998; Poore et al., 1999; Keigwin et al., 2006; Cronin et al., 2008) and obtained 18 new radiocarbon dates from the planktonic foraminifera species *Neogloboquadrina pachyderma* (Ehrenberg) within cores AOS94B8B, AOS94B20A, AOS94B26B, and PS 2179–3 (Table 3). All 199 radiocarbon dates are available online at the National Climatic Data Center: http://www.ncdc.noaa.gov/paleo/paleo.html. Dates were recalibrated using the CALIB 6.0 program with the MARINE09 402-year reservoir correction curve (Stuiver and Reimer, 2010). In addition to the global marine correction of 402 years, we followed Hanslik et al. (2010) and used an additional ΔR regional correction of 300 years for radiocarbon ages <10 ka, and a ΔR of 1000 years for ages >10 ka. Fig. 2 shows the age distribution of the 199 recalibrated radiocarbon dates from Arctic cores. There are 64 dates from within glacial MIS 3 (~50–29 ka) and 109 dates from the deglacial through the Holocene interglacial in MIS 1 (~15 ka-present), and only 15 dates from glacial MIS 2 (Fig. 2). The lack of MIS 2 radiocarbon dates in the Arctic Ocean agrees with previous studies that suggest little to no sedimentation in the central Arctic Ocean during the Last Glacial Maximum (LGM: ~22 ka ± 2 kyr) due to thick ice cover (Nørgaard-Pederson et al., 2003; Polyak et al., 2004, 2009; Hanslik et al., 2010). The average two standard-deviation error on calibrated ages older than 40 ka was ± 1.648 years; for ages 39 ka to 20 ka, ± 1003 years; and ages 20 ka to recent ± 199 years. A total of eleven dates had infinite ages (including some published radiocarbon ages of >40 ka) that were not used in the construction of our age models.

### 3.2. Composite Arctic faunal curves

Composite ("stacked") abundance curves were constructed for each of the five taxa to illustrate faunal changes in the intermediate to deep central Arctic Ocean, on the whole (Gakkel, Lomonosov, and Mendeleev Ridges), and to correlate these changes in the central Arctic with other paleoclimate records. These composites were constructed by averaging the abundances of each taxon from samples in the 15 studied cores from within the intermediate to deep water depths (~1000 to 3000 m) (AOS94B8B, AOS94B12A, AOS94B16C, AOS94B17B, AOS94B19B, AOS94B20A, AOS94B26B, AOS94B28B, PS 2163–1, PS 2179–3, PS 2184–3, PS 2185–4, PS 2186–3, PS 2206–4, and HLY0503-18tc), and binning them into 1000-yr time periods (i.e. 0–1 ka, 1–2ka, etc.). Samples with ≤30 specimens (39 of 421 samples) were excluded from the stacked composite data, to avoid statistical bias (samples used contained 282 specimens on average). The remaining six cores (AOS94B23A, AOS94B32, PS 2170–4, PS 2178–4, PS 2200–4, and PS 2202–4) were not included in the composite because the faunal zones (discussed below) were not as evident, likely due to the sites being within abyssal plain water depths (>3500 m), or located on the shallow continental margin of the Morris Jesup Rise (Fig. 1).

## 4. Results

Data from three cores from the Mendeleev Ridge (AOS94B8B, AOS94B16C, and AOSB19B) (Fig. 3) and three cores from the Lomonosov Ridge (AOS94B28B, PS 2186–3, and HLY0503-18tc) (Fig. 4) show typical patterns for their respective regions (all faunal data available online at the National Climatic Data Center: http://www.ncdc.noaa.gov/paleo/paleo.html). Four distinct ostracode zones can be recognized on the Mendeleev and Lomonosov Ridges. These zones will be referred to as (oldest to youngest): the *Krithe/Henryhowella* (KH) zone, the *Polycope* (P) zone, the *Cytheropteron/Krithe* (CK) zone, and the *Krithe/Acetabulastoma* (KA) zone.

The *Krithe/Henryhowella* (KH) zone typically shows relatively high abundances of *H. asperrima* (~10–80%), *Krithe* spp. (~5–60%), and *Cytheropteron* spp. (~10–60%). The KH zone corresponds to *Cytheropteron* spp. Maximum 1 (CM1), *H. asperrima* Maximum 1 (HM1), and *Krithe* spp. Maximum 1 (KM1), as described by Cronin et al. (1995). There are relatively low abundances of *Polycope* spp., and variable *A. arcticum* (~0–10%) from core to core within this zone (Figs. 3A, E and 4A, E; Table 4).

The *Polycope* (P) zone, is characterized by the dominance of *Polycope* spp. (~40–80%) (Figs. 3E and 4E) and corresponds to the *Polycope* Maximum 1 of Cronin et al. (1995). Abundances of *Cytheropteron* spp., *H. asperrima*, and *Krithe* spp. are significantly lower than in other zones, and *A. arcticum* is highly variable within this zone (Figs. 3A, B, C, D and 4A, B, C, D; Table 4).

The *Cytheropteron/Krithe* (CK) zone shows a decreased abundance of *Polycope* spp. (~0–40%) with peaks of *Cytheropteron* spp. (~20–60%), *Krithe* spp. (~5–90%) and to a lesser extent *H. asperrima* (~0–30%) (Figs. 3B, C, D, E and 4B, C, D, E). The abundance of *A. arcticum* increases in some cores (~3–7%), but remains low in others (~0-2%) (Figs. 3A and 4A; Table 4). The CK zone corresponds to *Cytheropteron* Maximum 2 (CM2) and the end of PM1 of Cronin et al. (1995).

The *Krithe/Acetabulastoma* (KA) zone is characterized by peaks of *Krithe* spp. (~10–90%) and significant numbers (~5–10%) of *A. arcticum* (Figs. 3A, C and 4A, C). It includes *A. arcticum* Maximum 1 (AM1), *Cytheropteron* spp. Maximum 3 (CM3), *H. asperrima* Maximum 2 (HM2), and *Krithe* spp. Maximum 2 (KM2) of Cronin et al. (1995). Samples from the KA zone in some cores contained varying amounts of *Polycope* spp. (~15–70%) (Figs. 3E and 4E; Table 4).

Several regional differences could be observed in cores from the Mendeleev, Lomonosov and Gakkel Ridges (Figs. 3 and 4). For

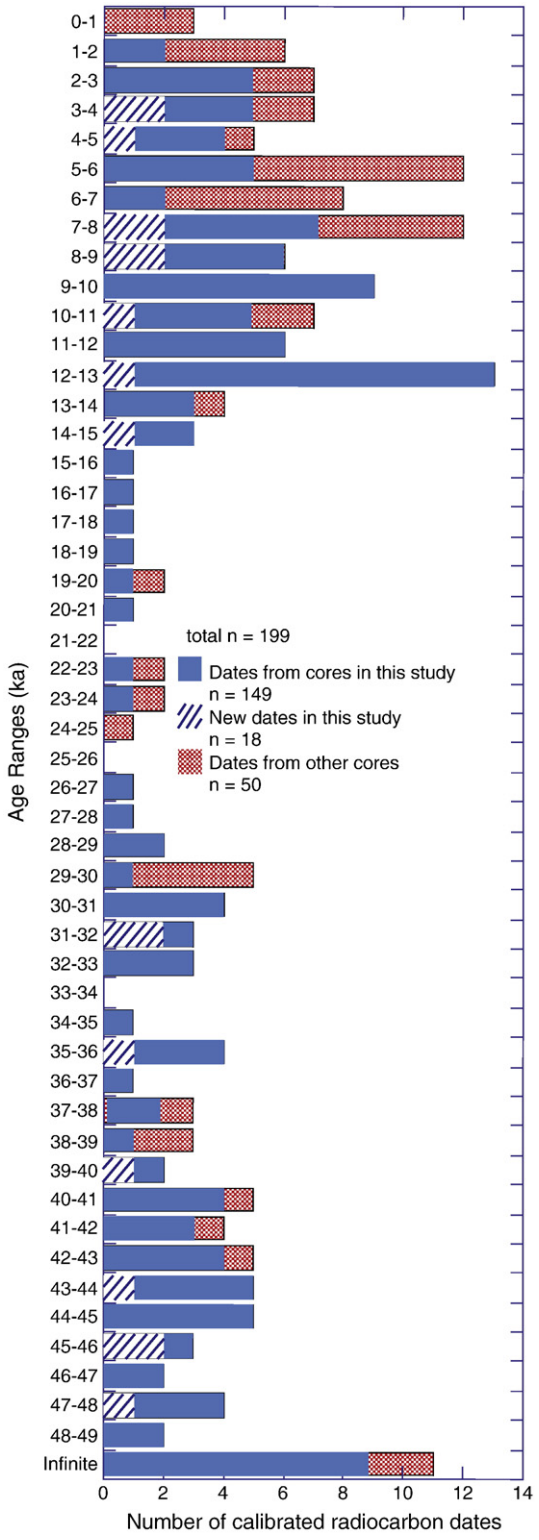


**Fig. 2.** Histogram of radiocarbon dates calibrated by the methodology of Hanslik et al. (2010). See Table 2 for radiocarbon dates.

example, the onset of the P-zone may have occurred earlier on average in the Mendeleev Ridge cores (~42 ka) than in the Lomonosov Ridge cores (~37 ka). Also, peaks of *Cytheropteron* spp., *H. asperrima*, and *Krithe* spp. during the KH zone from the Mendeleev Ridge cores appear to be of smaller scale (*Cytheropteron* spp.: 40–50%; *H. asperrima*: 10–35%; *Krithe* spp.: 5–45%) than those within the Lomonosov Ridge cores (*Cytheropteron* spp.: 30–60%; *H. asperrima*: 40–80%; *Krithe* spp.: 20–60%) (see Discussion below).

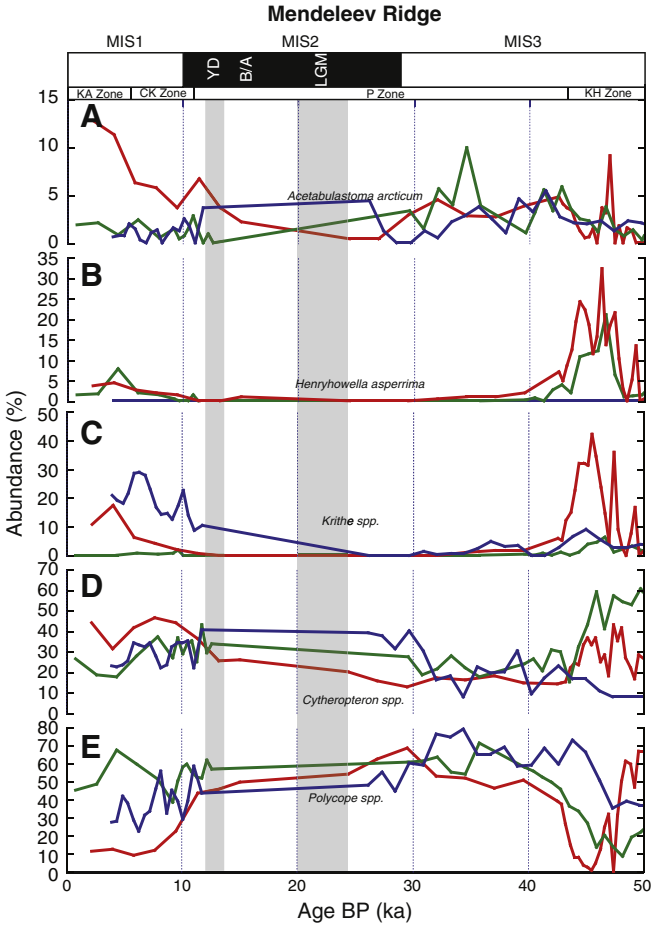


**Fig. 3.** Abundance (%) vs. age BP (kyr) for *Acetabulastoma arcticum* (A) *Henryhowella asperrima* (B) *Krithe* spp. (C) *Cytheropteron* spp. (D) and *Polycope* spp. (E), from three cores on the Mendeleev Ridge: AOS94B8B (blue), AOS94B16C (green), and AOS94B19B (red) with approximation location of the Last Glacial Maximum (LGM), Bølling–Allerød (B/A), and Younger Dryas (YD). (For interpretation of the references to color in this figure legend, the reader is referred to the web version of this article.)

### 4.1. Composite Arctic faunal curves

The stacked composite faunal curves in Fig. 5 illustrate the faunal zones discussed above and their approximate age ranges for the central Arctic region: KH zone: ~50–38 kyr BP; P zone: ~38–18 kyr BP; CK zone: ~18–7 kyr BP; KA zone: ~7 kyr BP to present. The 95% confidence interval error bars for each 1000-yr interval suggest that ostracode assemblages illustrate significant large-scale faunal changes in the central Arctic during the last 50 kyr (Fig. 5).

Fig. 5 also compares the ostracode zones to the oxygen isotope curve of the NGRIP ice core from Greenland (Andersen et al., 2006; Rasmussen et al., 2006; Svensson et al., 2006, 2008; Vinther et al., 2006). DO events 1 (the Bølling–Allerød) through 13 are labeled, based on the description of Dansgaard et al. (1984, 1993) and the updated chronology of Andersen et al. (2006), Rasmussen et al. (2006), Svensson et al. (2006, 2008) and Vinther et al. (2006) (Fig. 5). Heinrich (H) event 0 (the Younger Dryas) through H-5 are also shown by vertical highlighted areas, and are based on ages from Hemming (2004), Wang et al. (2006), and Stanford et al. (2011).

The following tentative correlations between the ostracode faunal changes and DO and H-events are proposed: peak abundances of *Cytheropteron* spp., *H. asperrima*, and *Krithe* spp. during major DO events (notably DO 1, 3–4, 5–7, 8, and 12), the deglacial, and the interglacial; *Polycope* spp. abundance peaks during major H-events (notably 1–5, and potentially H-0), and the glacial; high *A. arcticum* abundance within the mid-late Holocene, and the period of time

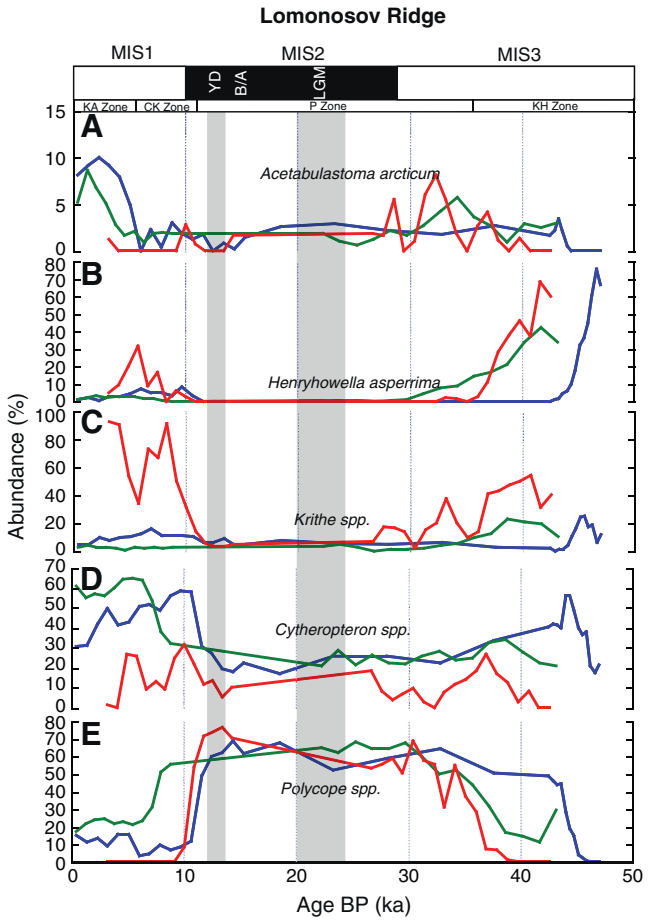


**Fig. 4.** Abundance (%) vs. age BP (kyr) for *Acetabulastoma arcticum* (A) *Henryhowella asperrima* (B) *Krithe* spp. (C) *Cytheropteron* spp. (D) and *Polycope* spp. (E), from three cores on the Lomonosov Ridge: AOS94B28B (blue), PS 2186–3 (green), and HLY0503-18tc (red) with approximation location of the Last Glacial Maximum (LGM), Bølling–Allerød (B/A), and Younger Dryas (YD). (For interpretation of the references to color in this figure legend, the reader is referred to the web version of this article.)

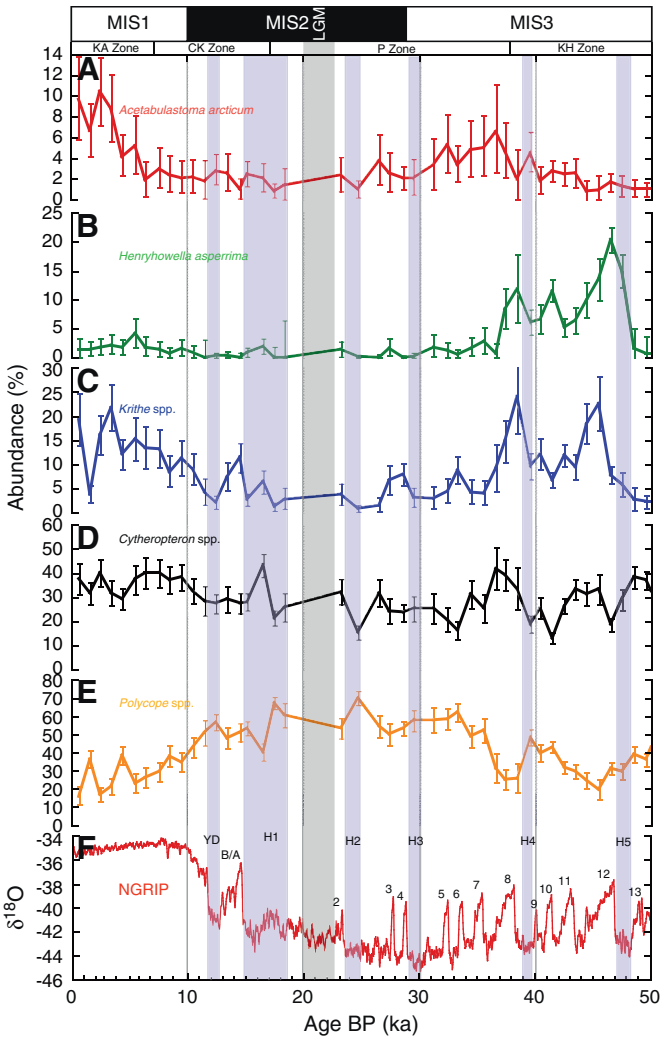


**Fig. 5.** Composite abundance (%) vs. age BP (kyr) for *Acetabulastoma arcticum* (A) *Henryhowella asperrima* (B) *Krithe* spp. (C) *Cytheropteron* spp. (D) and *Polycope* spp. (E), from 15 cores, showing ostracode zones. NGRIP ice cores oxygen isotope curve (F) from (Andersen et al., 2006; Rasmussen et al., 2006; Svensson et al., 2006, 2008; Vinther et al., 2006). Heinrich (H) events 5–1, Dansgaard–Oeschger (DO) events 13–2, the Younger Dryas (YD; H0), the Bølling–Allerød (B/A; DO-1), are labeled.

including major DO events 3–8, during mid-late MIS 3 and early MIS 2 (Fig. 5).

### 4.2. Contrast between MIS 1 interglacial and MIS 3 glacial conditions

In order to illustrate the contrast between deep Arctic faunas in the modern Arctic Ocean, the Holocene interglacial (MIS 1), and stadial conditions of MIS 3/2 (~20 to 40 ka), we constructed cross sections of abundances using Ocean Data View. Figs. 6A and 7A illustrate the abundances of *Krithe* spp. and *Polycope* spp. in the modern Arctic from the Modern Arctic Ostracode Database (MAOD) ftp://ftp.ncdc.noaa.gov/pub/data/paleo/contributions_by_author/cronin2010/cronin2010.txt (Cronin et al., 2010), compared to those during MIS 1 (samples from the last ~10 ka) (Figs. 6B and 7B), and those within the stadially-dominated period of MIS 3/2 (between ~20 and 40 ka) (Figs. 6C and 7C). The modern distribution of *Krithe* suggests highest abundances (10 to 70%) within the AODW at water depths below ~2000 m (Fig. 6A). Similarly, the distribution of *Krithe* from the interglacial Holocene shows that the taxon occurred in highest abundances (~10 to 80%) at relatively deep water-depths (~2000-3500 m) (Fig. 6B). *Krithe* typically occurs in highest abundances in the AODW in the central Arctic Ocean, and lowest in the AIW and/or the AL. In contrast, the abundances of

**Table 4**
Summary table of ostracode zones (KH, P, CK, and KA), dominant taxa for each, and zonal age ranges.

| Ostracode zone | Zone abbreviation | Canada Basin age range (ka) | Eurasian Basin age range (ka) | Central Arctic age range (ka) | Dominant taxa | |
|---|---|---|---|---|---|---|
| | | | | | Name: | Indicator of: |
| *Krithe/Acetabulastoma* zone | KA-zone | ~6 to present | ~9 to present | ~7 to present | *Krithe* spp.<br>*Acetabulastoma arcticum* | cold, well-ventilated AODW<br>perennial sea ice |
| *Cytheropteron/Krithe* zone | CK-zone | ~18 to 6 | ~11 to 9 | ~18 to 7 | *Cytheropteron* spp.<br>*Krithe* spp. | AIW/AODW<br>cold, well-ventilated AODW |
| *Polycope* zone | P-zone | ~42 to 18 | ~37 to 11 | ~38 to 18 | *Polycope* spp. | low productivity, AL influence |
| *Krithe/Henryhowella* zone | KH-zone | ~50 to 42 | ~50 to 37 | ~50 to 38 | *Krithe* spp.<br>*Henryhowella asperrima* | cold, well-ventilated AODW<br>cold, well-ventilated AODW |

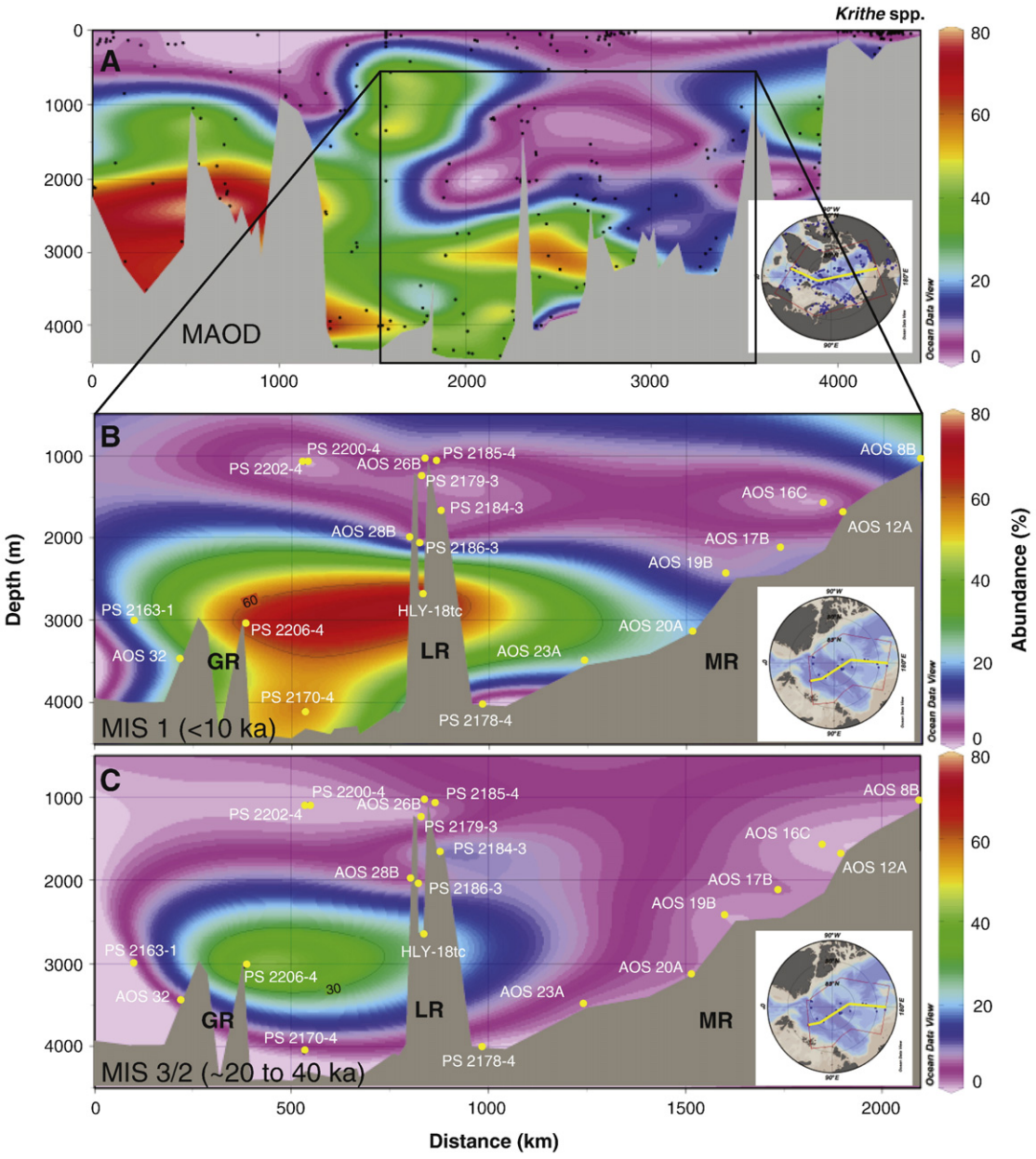


**Fig. 6.** A: Arctic cross section showing the modern abundances of *Krithe* spp. in surface sediment samples (mostly coretops). Data taken from the Modern Arctic Ostracode Database (MAOD). B: Average abundances of *Krithe* spp. during MIS1 (<10 kyr) from this study. C: Average abundances of *Krithe* spp. during MIS 3/2 (~20 to 40 ka).

*Krithe* during MIS 3/2 are much lower (~10 to 40%) at depths of ~2000 to 4000 m. *Krithe* is not as common during MIS 3/2, primarily limited to the region between the Gakkel and Lomonosov Ridges (Fig. 6B, C).

The modern distribution of *Polycope* shows highest abundances (~40 to 60%) between ~800 and 2000 m water depth (Fig. 7A). This suggests that today this taxon occurs in the AL and the AIW (Fig. 1), a pattern similar to that during the Holocene (Fig. 7B). During MIS 3/2, *Polycope* had high abundances (~30 to 80%) and its depth distribution expanded significantly to water depths from ~1000 m to 3000 m in the Makarov Basin and ~3000 and 4000 m in the Nansen Basin (Fig. 7C). The only areas where *Polycope* was rare (<10%) during MIS 2 were the deep Amundsen Basin below ~3000 m, and the deep Makarov Basin below ~3500 m (Fig. 7C).

## 5. Discussion

These analyses suggest that there were major faunal differences in the Arctic Ocean between interglacial and glacial regimes, and also between larger interstadial and stadial oscillations during the last 50 kyr. *Cytheropteron* spp., *H. asperrima*, and *Krithe* spp. dominate faunal assemblages during the Holocene interglacial period (MIS 1) and interstadial events, while *Polycope* spp. dominates the glacial period (MIS 2) and stadial events. The differences between warm and cool climate states imply large changes in intermediate and deep-water Arctic water masses occurred during the last 50 kyr.

The Holocene interglacial and interstadial assemblages from sediments correlating with DO 12 and DO 8, and the Bølling–Allerød, suggest oceanographic conditions at these times were similar to those in the modern Arctic Ocean. The Arctic was probably well-stratified and ventilated (~6 to 7 ml/l oxygen) beneath the AL. Therefore, similar conditions to the modern can be hypothesized during the interglacial Holocene, and large DO interstadial events. These interstadial events during MIS 3 may correlate with the High Productivity (HP) zones described by Hald et al. (2001) in which strong Atlantic water inflow characterized regions at shallower depths near Svalbard. For example Hald et al. (2001) noted the

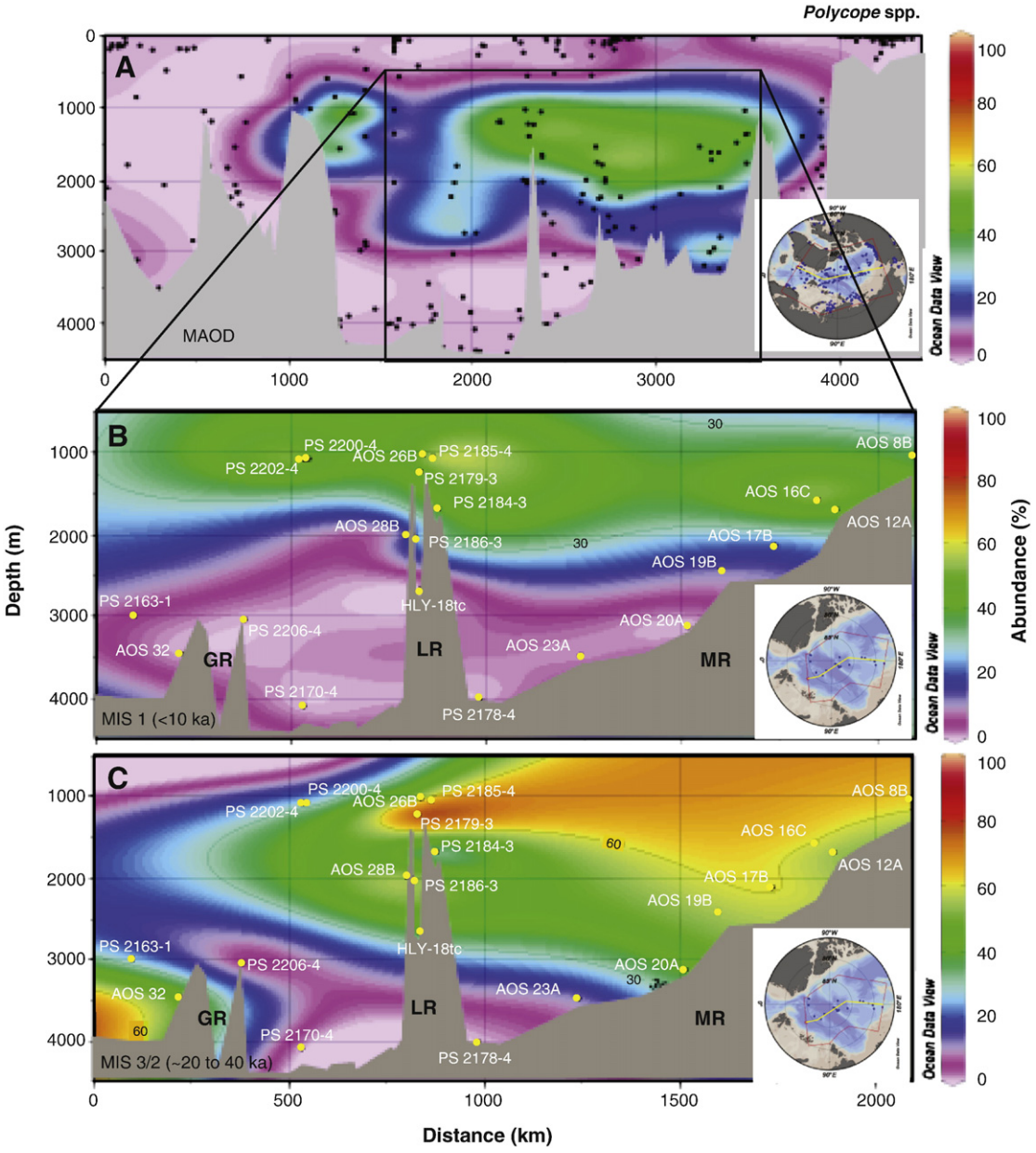


**Fig. 7.** A: Arctic cross section showing the modern abundances of *Polycope* spp. in surface sediment samples (mostly coretops). Data from the Modern Arctic Ostracode Database (MAOD). B: Average abundances of *Polycope* spp. during MIS1 (<10 kyr), from this study. C: Average abundances of *Polycope* spp. during MIS 3/2 (~20 to 40 ka).

following high productivity (HP) zones: HP-1 (~14.5 to 19.5 ka), HP2 (~22.5 to 29 ka), HP3 (~35 to 37.5 ka), HP-4 (~45 to 47 ka), and HP-5 (~49 to 51 ka). Backman et al. (2009) show peaks in calcareous nannoplankton in central Arctic core HLY0503-18tc at 40 to 60 cm core depth coincident with our KH ostracode zone between 45 and 60 cm. Ostracode faunas indicating interstadial conditions during this interval (the *Krithe–Henryhowella* assemblage) and the near absence of the sea-ice species *A. arcticum* support the nannofossil data of Backman et al. (2009) showing at least intermittently sea-ice free conditions in the central Arctic during this time. Well-oxygenated and stratified Arctic deep-water during the interglacial Holocene (MIS 1) and interstadial events is also consistent with results from van Kreveld et al. (2000) who determined that interstadial events are characterized by both strong ventilation and circulation in the Irminger Sea near Iceland.

In contrast, the dominance of *Polycope* between ~1000 and 3000 m during stadial events suggests greater influence of the AL and warmer temperatures at intermediate to deep sites, the entrainment of warmer water to greater depths, and a distinctive mode of Arctic intermediate and deep-water circulation. Although the mechanisms that might produce a warm, deep Arctic Ocean water mass are not clear, there is evidence for large ocean circulation change during stadial events and glacial periods. For example, evidence for increased brine formation in the North Atlantic during H3 and H4, was noted by Vidal et al. (1998) with a regional influence of $\delta^{18}O$ -depleted (benthic) meltwater to greater depths during periods of iceberg discharge. Polyak et al. (2004) concluded that faunal-poor layers in Arctic sediments, with suppressed biological production corresponding to major glaciations, indicate extremely thick pack ice or ice shelves covered the western Arctic Ocean, and that Arctic circulation was restricted, with reduced bottom water formation. Spielhagen et al. (2004) noted that during major glacial periods of the last 200 kyrs the Arctic was characterized by large amounts of coarse, terrigenous ice-rafted debris (IRD) and smaller amounts of bioproductive sediments. Analyses of benthic foraminifera from the Yermak Plateau, Arctic Ocean, by Wollenburg et al. (2004), suggest that during the LGM, paleoproductivity was reduced to a third of its present level. Hald et al. (2001) suggested more sluggish

circulation and year-round sea-ice cover during zones of minimal bioproductivity during stadials from core sites near Svalbard. Thicker sea-ice or ice shelves during stadials could have forced the Atlantic water's influence deeper in the Arctic through the Fram Strait. Additionally, van Kreveld et al. (2000) hypothesized that abundant brine formation entrained warmer water in the Irminger Sea during stadial events, accompanied by weakened thermohaline circulation. Dokken and Jansen (1999) suggested that during stadial events, the mode of thermohaline water mass convection in the Nordic Seas shifted to one dominated by brine formation. Bauch and Bauch (2001) concluded that entrainment of waters with low $\delta^{18}O$ could have occurred via glacial meltwater below an ice shelf and brine release by sea-ice formation in the deep-waters of the Nordic Seas, contributing to those of the Arctic Ocean. Rasmussen et al. (2007) noted an increase of 'Atlantic' species in benthic foraminiferal assemblages on the Svalbard margin during H1. Taken together with our ostracode data, it is possible that a warmer, less productive water mass formed either within or outside the Arctic proper, and influenced the Arctic Ocean between ~1000 and 3000 m water depth during the last glacial period (MIS 2) and during MIS 3 stadial events.

Although additional cores with multiple sea-ice proxies are needed, the low *A. arcticum* abundances during the KH-zone interstadial period, the deglacial, and early Holocene interglacial (MIS 1) indicate lower mean sea-ice conditions than during stadial/glacial periods. This interpretation coincides with the findings of Cronin et al. (2010) who found minimal sea ice during the early Holocene thermal maximum (8 to 5 ka) and the last deglacial (16–11 ka). Polyak et al. (2010) also concluded there was less sea-ice in the Arctic during Quaternary interglacials and major interstadial events. Although relatively few radiocarbon dates are available for the LGM, it was likely a period with substantially thicker sea-ice, possibly ice shelves (Polyak et al., 2004, 2010; Spielhagen et al., 2004; Jakobsson et al. 2010), and reduced bioproduction in the central Arctic Ocean (Nørgaard-Pederson et al., 2003; Backman et al., 2009). Additionally, the low abundances of *Acetabulastoma arcticum* during the more prominent stadial events of MIS 2 may represent a time when the sea-ice was so thick, that no suitable habitat for the pelagic amphipods, on which it lived, existed (Fig. 5).

## 6. Conclusions

Using ostracode assemblages to reconstruct paleoceanographic conditions in the central Arctic, we determined that the major water masses experienced large-scale changes throughout the last 50 kyr, alternating between sluggish, poorly ventilated stadial (glacial) periods (*Polycope* (P) zone) and well-stratified, ventilated interstadial and interglacial periods, (*Krithe/Henryhowella* (KH), *Cytheropteron/Krithe* (CK), and *Krithe/Acetabulastoma* (KA) zones). These changes were probably related to variable sea-ice thickness, ice shelves, as well as the strength and location of deep-water formation probably outside the Arctic proper.

## Acknowledgments

Thanks to Dr. E. Brouwers, R. Kihl, C. Callicott, T. Nettleton, N. Seevers, and T. Ichinose for sample processing, to Dr. S. Holland (University of Georgia) who publicly provided his 95% confidence error bars program, to R. Marzen for Ocean Data View graphics help, and to M. Robinson, J. Self-Trail, J. Farmer, and two anonymous reviewers for useful comments. This work is funded by USGS Global Change Program; WMB Jr. was funded by National Science Foundation Grant OPP-9400255.

## Appendix A. Supplementary data

Supplementary data to this article can be found online at doi:10.1016/j.marmicro.2012.03.004.

## References

Aagaard, K., Carmack, E.C., 1989. The role of sea ice and other fresh water in the Arctic circulation. Geophysical Research 9 4 (14), 485–498.
Aagaard, K., Carmack, E.C., 1994. The Arctic and climate: a perspective in Polar Oceans and their role in shaping the global environment. : Geophysical Monograph Series. American Geophysical Union, Washington, D.C., pp. 4–20.
Aagaard, K., Swift, J.H., Carmack, E.C., 1985. Thermohaline circulation in the Arctic Mediterranean Seas. Journal of Geophysical Research 90, 4833–4846.
Aagaard, K., Fahrback, E., Meincke, J., Swift, J.H., 1991. Saline outflow from the Arctic Ocean: its contribution to deep waters of the Greenland, Norwegian, and Iceland Seas. Journal of Geophysical Research 96 (20), 433–441.
Andersen, K.K., Svensson, A., Johnsen, S.J., Rasmussen, S.O., Bigler, M., Rothlisberger, R., Ruth, U., Siggaard-Andersen, M.-L., Steffensen, J.P., Dahl Jensen, D., Vinther, B.M., Clausen, H.B., 2006. The Greenland Ice Core Chronology 2005, 15–42 ka. Part 1: constructing the time scale. Quaternary Science Reviews 25, 3246–3257. doi:10.1016/j.quascirev.2006.08.002.
Anderson, L.G., Jones, E.P., 1992. Tracing upper waters in the Nansen Basin in the Arctic Ocean. Deep Sea Research 39 (Suppl. 2), 425–433.
Anderson, L.G., Bjork, G., Holby, O., Jones, E.P., Kattner, G., Koltemann, K.P., Liljeblad, B., Lindegren, R., Rudels, B., Swift, J., 1994. Water masses and circulation in the Eurasian Basin: results from the *Oden* 91 North Pole Expedition. Journal of Geophysical Research 99, 3273–3283.
Andrews, J.T., 1998. Abrupt changes (Heinrich events) in late Quaternary North Atlantic marine environments: a history and review of data and concepts. Journal of Quaternary Science 13, 3–16.
Backman, J., Fornaciari, E., Rio, D., 2009. Biochronology and paleoceanography of late Pleistocene and Holocene nannofossil abundances across the Arctic Basin. Marine Micropaleontology 72, 86–98.
Bauch, D., Bauch, H.A., 2001. Last glacial benthic foraminiferal $\delta^{18}O$ anomalies in the polar North Atlantic: a modern analogue evaluation. Journal of Geophysical Research 106 (C5), 9135–9143.
Bond, G., Heinrich, H., Broecker, W., Labeyrie, L., McManus, J., Andrews, J., Huon, S., Jantschik, R., Clasen, S., Simit, C., Tedesco, K., Klas, M., Bonani, G., Ivy, S., 1992. Evidence for massive discharges of icebergs into the North Atlantic Ocean during the last glacial period. Nature 360, 245–249.
Bourke, R.H., Weigel, A.M., Paquette, R.G., 1988. The westward turning branch of the West Spitsbergen Current. Journal of Geophysical Research 93, 14,065–14,077.
Clark, P.U., Pisias, N.G., Stocker, T.F., Weaver, A.J., 2002. The role of the thermohaline circulation in abrupt climate change. Nature 415, 863–869.
Comiso, J.C., Parkinson, C.L., Gersten, R., Stock, L., 2008. Accelerated decline in the Arctic Sea ice cover. Geophysical Research Letters 35, L01703. doi:10.1029/2007GL03.
Cronin, T.M., Holtz Jr., T.R., Whatley, R.C., 1994. Quaternary paleoceanography of the deep Arctic Ocean based on quantitative analysis of Ostracoda. Marine Geology 119, 305–332.
Cronin, T.M., Holtz Jr., T.R., Stein, R., Spielhagen, R., Futterer, D., Wollenburg, J., 1995. Late Quaternary paleoceanography of the Eurasian Basin, Arctic Ocean. Paleoceanography 10 (2), 259–281.
Cronin, T.M., Smith, S.A., Eynaud, F., O'Regan, M., King, J., 2008. Quaternary paleoceanography of the central Arctic based on Integrated Ocean Drilling Program Arctic Coring Expedition 302 foraminiferal assemblages. Paleoceanography 23, PA1S18. doi:10.1029/2007PA001484.
Cronin, T.M., Gemery, L., Briggs Jr., W.M., Jakobsson, M., Polyak, L., Brouwers, E.M., 2010. Quaternary sea-ice history in the Arctic Ocean based on a new ostracode sea-ice proxy. Quaternary Science Reviews 29, 3415–3429. doi:10.1016/j.quascirev.2010.05.024.
Dansgaard, W., Johnsen, S.J., Clausen, H.B., 1984. North Atlantic climatic oscillations revealed by deep Greenland ice cores. Climate Processes and Climate Sensitivity. American Geophysical Union, pp. 288–298.
Dansgaard, W., Johnsen, S.J., Clausen, H.B., Dahl-Jensen, D., Gundestrup, N.S., Hammer, C.U., Hvidberg, C.S., Steffensen, J.P., Sveinbjornsdottir, A.E., Jouzel, J., Bond, G., 1993. Evidence for general instability of past climate from a 250 kyr ice-core record. Nature 364, 218–220.
Darby, D.A., Bischof, J.F., Jones, G.A., 1997. Radiocarbon chronology of depositional regimes in the western Arctic Ocean. Deep Sea Research 44 (8), 1745–1757.
Darby, D., Polyak, L., Bauch, H.A., 2006. Past glacial and interglacial conditions in the Arctic Ocean and marginal seas—a review. Progress in Oceanography 71, 129–144.
Dokken, T.M., Jansen, E., 1999. Rapid changes in the mechanism of ocean convection during the last glacial period. Nature 401, 458–461.
Elliot, M., Labeyrie, L., Duplessy, J.-C., 2002. Changes in North Atlantic deep-water formation associated with the Dansgaard–Oeschger temperature oscillations (60–10 ka). Quaternary Science Reviews 21, 1153–1165.
Hald, M., Dokken, T., Mikalsen, G., 2001. Abrupt climatic change during the last interglacial–glacial cycle in the polar North Atlantic. Marine Geology 176, 121–137.
Hanslik, D., Jakobsson, M., Backman, J., Bjorck, S., Sellen, E., O'Regan, M., Fornaciari, E., Skog, G., 2010. Quaternary Arctic Ocean sea ice variations and radiocarbon reservoir age corrections. Quaternary Science Reviews 29, 3430–3441.
Heinrich, H., 1988. Origin and consequences of cyclic ice rafting in the northeast Atlantic Ocean during the past 130,000 years. Quaternary Research 29, 143–152.
Hemming, S.R., 2004. Heinrich events: Massive late Pleistocene detritus layers of the North Atlantic and their global climate imprint. Reviews of Geophysics 42, 1–43.
Jakobsson, M., Lovlie, R., Arnold, E.M., Backman, J., Polyak, L., Knutsen, J.-O., Musatov, E., 2001. Pleistocene stratigraphy and paleoenvironmental variation from Lomonosov Ridge sediments, central Arctic Ocean. Global and Planetary Change 31 (1–4), 1–22.
Jakobsson, M., Macnab, R., Mayer, L., Anderson, R., Edwards, M., Hatzky, J., Schenke, H.W., Johnson, P., 2008. An improved bathymetric portrayal of the Arctic Ocean: implications for ocean modeling and geological, geophysical and oceanographic analyses. Geophysical Research Letters 35. doi:10.1029/2008GL033520.

Jakobsson, M., Long, A., Ingolfsson, O., Kjaer, K.H., Spielhagen, R., 2010. New insights on Arctic Quaternary climate variability from palaeo-records and numerical modeling. Quaternary Science Reviews 29 (25–26), 3349–3358.
Jones, E.P., 2001. Circulation in the Arctic Ocean. Polar Research 20 (2), 139–146.
Jones, E.P., Rudels, B., Anderson, L.G., 1995a. Deep waters of the Arctic Ocean: origins and circulation. Deep Sea Research 42, 737–760.
Jones, E.P., Rudels, B., Anderson, L.G., 1995b. Deep waters of the Arctic Ocean: origins and circulation. Deep Sea Research 42 (5), 737–760.
Jones, R.L., Whatley, R.C., Cronin, T.M., 1998. The zoogeographical distribution of deep water Ostracoda in the Arctic Ocean. In: Sylvie Crasquin, S., Braccini, E., Lethiers, F. (Eds.), What about Ostracoda! Third European Ostracodologists Meeting, Paris-Bierville, 2996. Elf Exploration Production Editions, Pau, pp. 83–90.
Jones, R.L., Whatley, R.C., Cronin, T.M., Dowsett, H.J., 1999. Reconstructing late Quaternary deep-water masses in the eastern Arctic Ocean using benthonic Ostracoda. Marine Micropaleontology 37, 251–272.
Joy, J.A., Clark, D.L., 1977. The distribution, ecology and systematics of the benthic Ostracoda of the Central Arctic Ocean. Micropaleontology 23 (2), 129–154.
Karcher, M.J., Oberhuber, J.M., 2002. Pathways and modification of the upper and intermediate waters of the Arctic Ocean. Journal of Geophysical Research 107 (C6), 3049. doi:10.1029/2000JC000530.
Kaufman, D.S., Ager, T.A., Anderson, N.J., Anderson, P.M., Andrews, J.T., Bartlein, P.J., Brubaker, L.B., Coats, L.L., Cwynar, L.C., Duvall, M.L., Dyke, A.S., Edwards, M.E., Eisner, W.R., Gajewski, K., Geirsdottir, A., Hu, F.S., Jennings, A.E., Kaplan, M.R., Kerwin, M.W., Lozhkin, A.V., MacDonald, G.M., Miller, G.H., Mock, C.J., Oswald, W.W., Otto-Bliesner, B.L., Porinchu, D.F., Ruhland, K., Smol, J.P., Steig, E.J., Wolfe, B.B., 2004. Holocene thermal maximum in the western Arctic (0–180°W). Quaternary Science Reviews 23, 529–560.
Keigwin, L.D., Lehman, S.J., 1994. Deep circulation change linked to Heinrich event 1 and Younger Dryas in a mid-depth North Atlantic core. Paleoceanography 9, 185–194.
Keigwin, L.D., Donnelly, J.P., Cook, M.S., Driscoll, N.W., Brigham-Grette, J., 2006. Rapid sea-level rise and Holocene climate in the Chukchi Sea. Geology 34 (10), 861–864.
Kwok, R., Rothrock, D.A., 2009. Decline in Arctic sea ice thickness from submarine and ICESat records: 1958–2008. Geophysical Research Letters 36, L15501. doi:10.1029/2009GL039035.
McCartney, M.S., Talley, L.D., 1984. Warm-to-cold water conversions in the northern North Atlantic Ocean. Journal of Physical Oceanography 14, 922–935.
McLaughlin, F.A., Carmack, E.C., Williams, W.J., Zimmermann, S., Shimada, K., Itoh, M., 2009. Joint effects of boundary currents and thermohaline intrusions on the warming of Atlantic water in the Canada Basin, 1993–2007. Journal of Geophysical Research 114. doi:10.1029/2008JC005001.
Meincke, J., Rudels, B., Friedrich, H.J., 1997. The Arctic Ocean–Nordic Seas thermohaline system. ICES Journal of Marine Science 54, 283–299.
Nørgaard-Pederson, N., Spielhagen, R.F., Thiede, J., Kassens, H., 1998. Central Arctic surface ocean environment during the past 80,000 years. Paleoceanography 13 (2), 193–204.
Nørgaard-Pederson, N., Spielhagen, R.F., Erlenkeuser, H., Grootes, P.M., Heinemeier, J., Knies, J., 2003. Arctic Ocean during the Last Glacial Maximum: Atlantic and polar domains of surface water mass distribution and ice cover. Paleoceanography 18 (3), 1063. doi:10.1029/2002PA000781.
Polyak, L., Curry, W.B., Darby, D.A., Bischof, J., Cronin, T.M., 2004. Contrasting glacial/interglacial regimes in the western Arctic Ocean as exemplified by a sedimentary record from the Mendeleev Ridge. Palaeogeography, Palaeoclimatology, Palaeoecology 203 (1–2), 73–93.
Polyak, L., Bischof, J., Ortiz, J.D., Darby, D.A., Channell, J.E.T., Xuan, C., Kaufman, D.S., Løvlie, R., Schneider, D.A., Eberl, D.D., Adler, R.E., Council, E.A., 2009. Late Quaternary stratigraphy and sedimentation patterns in the western Arctic Ocean. Global and Planetary Change 68, 5–17.
Polyak, L., Alley, R.B., Andrews, J.T., Brigham-Grette, J., Cronin, T.M., Darby, D.A., Dyke, A.S., Fitzpatrick, J.J., Funder, S., Holland, M., Jennings, A.E., Miller, G.H., O'Regan, M., Savelle, J., Serreze, M., St. John, K., White, J.W.C., Wolff, E., 2010. History of sea ice in the Arctic. Quaternary Science Reviews 29, 1757–1778.
Polyakov, I.V., Alexeev, V.A., Ashik, I.M., Bacon, S., Beszczynska-Moller, A., Carmack, E.C., Dmitrenko, I.A., Forthier, L., Gascard, J.-C., Hansen, E., Holemann, J., Ivanov, V.V., Kikuchi, T., Kirillov, S., Lenn, Y.-D., McLaughlin, F.A., Piechura, J., Repina, I., Tiimokhov, L.A., Walczowski, W., Woodgate, R., 2011. Fate of Early 2000s Arctic Warm Water Pulse. American Meteorological Society. doi:10.1175/2010BAMS2921.1.
Poore, R.Z., Osterman, L., Curry, W.B., Philips, R.L., 1999. Late Pleistocene and Holocene meltwater events in the western Arctic Ocean. Geology 27 (8), 759–762.
Rasmussen, S.O., Andersen, K.K., Svensson, A.M., Steffensen, J.P., Vinther, B.M., Clausen, H.B., Siggaard-Andersen, M.-L., Johnsen, S.J., Larsen, L.B., Dahl Jensen, D., Bigler, M., Rothlisberger, R., Fischer, H., Goto-Azuma, K., Hansson, M.E., Ruth, U., 2006. A new Greenland ice core chronology for the last glacial termination. Journal of Geophysical Research 111 (D6), 1–16.
Rasmussen, T.L., Thomsen, E., Slubowska, M.A., Jessen, S., Solheim, A., Koc, N., 2007. Paleoceanographic evolution of the SW Svalbard margin (76°N) since 20,000 $^{14}$C yr BP. Quaternary Research 67, 100–114.
Raup, D.M., 1991. The future of analytical paleobiology. In: Gilinsky, N.L., Signor, P.W. (Eds.), Analytical Paleobiology: Paleontological Society Short Courses in Paleontology, 4, pp. 207–216.
Rothrock, D.A., Percival, D.B., Wensnahan, M., 2008. The decline in arctic sea-ice thickness: separating the spatial, annual, and interannual variability in a quarter century of submarine data. Journal of Geophysical Research 113, C05003. doi:10.1029//2007JC004252.
Rudels, B., 1987. On the mass balance of the Polar Ocean, with special emphasis on the Fram Strait. Norsk Polarinstitutt Skrifter 188, 53.
Rudels, B., Quadfasel, D., 1991. Convection and deep water formation in the Arctic Ocean–Greenland Sea system. Journal of Marine Systems 2, 435–450.
Rudels, B., Jones, E.P., Anderson, L.G., Kattner, G., 1994. On the intermediate depth waters of the Arctic Ocean. The Role of the Polar Oceans Shaping the Global Climate. American Geophysical Union, Washington, D.C., pp. 33–46.
Rudels, B., Anderson, L.G., Jones, E.P., 1996. Formation and evolution of the surface mixed layer and the halocline of the Arctic Ocean. Journal of Geophysical Research 101, 8807–8821.
Rudels, B., Jones, E.P., Schauer, U., Eriksson, P., 2004. Atlantic sources of the Arctic Ocean surface and halocline waters. Polar Research 23 (2), 181–208.
Sarnthein, M., Winn, K., Jung, S.J.A., Duplessy, J.C., Labeyrie, L., Erlenkeuser, H., Ganssen, G., 1994. Changes in East Atlantic Deepwater Circulation over the last 30,000 years: eight time slice reconstructions. Paleoceanography 9 (2), 209–267.
Spielhagen, R.F., Baumann, K.H., Erlenkeuser, H., Nowaczyk, R., Nørgaard Pedersen, N., Vogt, C., Weiel, D., 2004. Arctic Ocean deep-sea record of northern Eurasian ice sheet history. Quaternary Science Reviews 23, 1455–1483.
Spielhagen, R.F., Erlenkeuser, H., Siegert, C., 2005. History of freshwater runoff across the Laptev Sea (Arctic) during the last deglaciation. Global and Planetary Change 48, 187–207.
Spielhagen, R.F., Werner, K., Sorensen, S.A., Zamelczyk, K., Kandiano, E., Budeus, G., Husum, K., Marchitto, T.M., Hald, M., 2011. Enhanced modern heat transfer to the Arctic by warm Atlantic water. Science 331 (6016), 450–453.
Stanford, J.D., Rohling, E.J., Bacon, S., Roberts, A.P., Grousset, F.E., Bolshaw, M., 2011. A new concept for the paleoceanographic evolution of Heinrich event 1 in the North Atlantic. Quaternary Science Reviews 30, 1047–1066.
Stein, R., Grobe, H., Wahsner, M., 1994a. Organic carbon, carbonate, and clay mineral distributions in eastern central Arctic Ocean surface sediments. Marine Geology 119 (3–4), 269–285.
Stein, R., Schubert, C., Vogt, C., Futterer, D., 1994b. Stable isotope stratigraphy, sedimentation rates, and salinity changes in the Latest Pleistocene to Holocene eastern central Arctic Ocean. Marine Geology 199, 333–355.
Stepanova, A., Taldenkova, E., Bauch, H.A., 2003. Recent Ostracoda from the Laptev Sea (Arctic Siberia): species assemblages and some environmental relationships. Marine Micropaleontology 48, 23–48.
Stepanova, A., Taldenkova, E., Simstich, J., Bauch, H.A., 2007. Comparison study of the modern ostracod associations in the Kara and Laptev seas: ecological aspects. Marine Micropaleontology 63, 111–142.
Stepanova, A.Y., Taldenkova, E.E., Bauch, H.A., 2010. Arctic Quaternary ostracods and their use in paleoreconstructions. Paleontological Journal 44 (1), 41–48.
Stroeve, J., Holland, M.M., Meier, W., Scambos, T., Serreze, M., 2007a. Arctic sea ice decline: faster than forecast. Geophysical Research Letters 34. doi:10.1029/2007GL029703.
Stroeve, J., Serreze, M., Drobot, S., Gearheard, S., Holland, M., Maslanik, J., Meier, W., Scambos, T., 2007b. Arctic Sea Ice Extent Plummets in 2007. EOS, Transactions, American Geophysical Union 89 (2), 13–20.
Stuiver, M., Reimer, P., 2010. CALIB 6.0.1 Reservoir Corrections program. Available online at: http://calib.qub.ac.uk/calib/.
Svensson, A., Andersen, K.K., Bigler, M., Clausen, H.B., Dahl-Jensen, D., Davies, S.M., Johnsen, S.J., Muscheler, R., Rasmussen, S.O., Rothlisberger, R., Steffensen, J.P., Vinther, B.M., 2006. The Greenland Ice Core Chronology 2005, 15–42 ka. Part 2: comparison to other records. Quaternary Science Reviews 25, 3258–3267. doi:10.1016/j.quascirev.2006.08.003.
Svensson, A., Andersen, K.K., Bigler, M., Clausen, H.B., Dahl-Jensen, D., Davies, S.M., Johnsen, S.J., Muscheler, R., Parrenin, F., Rasmussen, S.O., Rothlisberger, R., Seierstad, I., Steffensen, J.P., Vinther, B.M., 2008. A 60,000 year Greenland stratigraphic ice core chronology. Climate of the Past 4, 47–57.
van Kreveld, S., Sarnthein, M., Erlenkeuser, H., Grootes, P., Jung, S., Nadeau, M.J., Pflaumann, U., Voelker, A., 2000. Potential links between surging ice sheets, circulation changes, and the Dansgaard–Oeschger cycles in the Irminger Sea, 60–18 kyr. Paleoceanography 15 (4), 425–442.
Vidal, L., Labeyrie, L., van Weering, T.C.E., 1998. Benthic $\delta^{18}$O records in the North Atlantic over the last glacial period (60–10 kyr): evidence for brine formation. Paleoceanography 13 (3), 245–251.
Vinther, B.M., Clausen, H.B., Johnsen, S.J., Rasmussen, S.O., Andersen, K.K., Buchardt, S.L., Dahl-Jensen, D., Seierstad, I.K., Siggaard-Andersen, M.-L., Steffensen, J.P., Svensson, A.M., Olsen, J., Heinemeir, J., 2006. A synchronized dating of three Greenland ice cores throughout the Holocene. Journal of Geophysical Research 111. doi:10.1029/2005JD006921.
Wang, X., Auler, A.S., Edwards, R.L., 2006. Interhemispheric anti-phasing of rainfall during the last glacial period. Quaternary Science Reviews 25, 3391–3403.
Whatley, R., Coles, G., 1987. The Late Miocene to Quaternary Ostracoda of Leg 94, Deep Sea Drilling Project. Revista Española de Micropaleontología 19, 33–97.
Whatley, R., Eynon, M., Moguilevsky, A., 1995. The depth distribution of Ostracoda from the Greenland Sea. Journal of Micropalaeontology 17, 15–32.
Wollenburg, J.E., Knies, J., Mackensen, A., 2004. High-resolution paleoproductivity fluctuations during the past 24 kyr as indicated by benthic foraminifera in the marginal Arctic Ocean. Palaeogeography, Palaeoclimatology, Palaeoecology 204, 209–238.
Woodgate, R.A., Aagaard, K., Swift, J.H., Smethie Jr., W.M., Falkner, K.K., 2007. Atlantic water circulation over the Mendeleev Ridge and Chukchi Borderland from thermohaline intrusions and water mass properties. Journal of Geophysical Research 112, C02005. doi:10.1029/2005JC003416.
Worthington, L.V., 1970. The Norwegian Sea as a Mediterranean basin. Deep Sea Research 17, 77–84.